Direct Simulation of Three-Dimensional Hypersonic Flow About Intersecting Blunt Wedges

M. Cevdet Celenligil*
Vigyan Research Associates, Inc., Hampton, Virginia
Graeme A. Bird†
University of Sydney, Sydney, Australia
and
James N. Moss‡
NASA Langley Research Center, Hampton, Virginia

The present paper reports on one of the initial applications of the general three-dimensional direct simulation Monte Carlo (DSMC) method for calculating rarefied flows. Hypersonic flow around two blunt wedges that intersect at a 90-deg angle has been studied, and results are obtained for the transitional flow regime encountered at 85 and 100-km altitudes with a re-entry velocity of 7.5 km/s. In the computations, a real-gas model that accounts for internal energies (rotational and vibrational) and chemical reactions (five species) is used. The results show that the disturbance field in front of the double-wedge body is larger than that produced by a single wedge, and that surface pressures and flow densities are higher near the wedge intersection, whereas surface heating and shear stresses are greater at locations removed from the corner. Dissociation is important at 85 km, and the atomic oxygen, atomic nitrogen, and nitric oxide concentrations have their largest values near the wedge intersection. Results also show that three-dimensional flow structure occurs only near the wedge corner, and the flow monotonically approaches the limiting two-dimensional wedge flow case in the spanwise direction. At locations sufficiently distant from the wedge intersection, the results are found to be in good agreement with those of the two-dimensional wedge flow obtained in previous studies. The calculations of this study indicate that the general three-dimensional DSMC simulations are well suited for determining higher-altitude flows with today's computers, but become prohibitive at lower altitudes for most applications.

Nomenclature

C_i = mass fraction of species i, ρ_i/ρ
Kn = Knudsen number
M = Mach number
$\bar{M}$ = molecular weight of mixture
p = pressure
$\dot{q}$ = heat flux
T = total temperature
T_{tr} = translational temperature
U = velocity in x-direction
X_i = mole fraction of species i
x,y,z = Cartesian coordinates
Δt_m = time increment used in computations
λ = mean free path
ρ = density
τ = shear stress parallel to the grid line in streamwise direction

Subscripts
i = ith species
∞ = freestream values

Presented as Paper 88-0463 at the AIAA 26th Aerospace Sciences Meeting, Reno, NV, Jan. 11-14, 1988; received May 5, 1988; revision received Aug. 30, 1988.

*Research Engineer. Member AIAA.
†Professor, Department of Aeronautical Engineering. Associate Fellow AIAA.
‡Research Engineer. Associate Fellow AIAA.

Introduction

THE direct simulation Monte Carlo (DSMC) technique of Bird[1] has proven to be a good numerical scheme for the simulation of rarefied hypersonic flow problems in the transitional flow regime.[2-5] Experiments conducted in laboratories with Knudsen numbers of 0.1-2.0[6,7] and flows around space vehicles at altitudes of 70-160 km[4,8] have been computed using the DSMC method and the results of the computations show reasonably good agreement with the available experimental data.

Even though the DSMC technique has been used for the last 25 years, until recently, efforts have been concentrated primarily on one-[9] and two-dimensional[4,7] applications due to their smaller requirement for computational time and memory. Typically, using a reasonably fast computer with around 500K words memory, a moderately complicated two-dimensional flow can be computed with a couple of hours of central processor unit (CPU) time. However, all flows encountered in real life are three-dimensional in nature (except for the ones carefully conducted in laboratory experiments), and it is necessary to develop three-dimensional codes to solve these three-dimensional problems. In principle, three-dimensional cases do not present any conceptual difficulties for the application of the DSMC method because even in two-dimensional and one-dimensional cases, the collisions are computed in three-dimensional space. Yet, the requirements for the computer memory and CPU time for a typical three-dimensional flow problem are between one and two orders of magnitude more than those for a two-dimensional problem. Consequently, until recently, very little has been done about the application of the DSMC technique to three-dimensional flow problems because of the lack of fast computational facilities. In the past, three-dimensional flows have been either approximated by two-dimensional or one-dimensional computations for simpler idealized geometries, or special three-dimensional programs have been developed to compute the flows around axisymmetric bodies at angle of incidence. Only since the mid-

1980's have some general three-dimensional codes been developed by various groups[10] using today's supercomputers such as the CRAY-XMP and the CRAY-2. {It should be noted that although today's supercomputers provide the memory required for a reasonable three-dimensional computation [e.g., CRAY-2 has 256M (M = 1 million) words memory and also, several virtual memory computers are available], a typical three-dimensional run is still very time-consuming and costly. Hopefully, this situation can be substantially improved by utilizing parallel processing capabilities of new computers.}.

At the NASA Langley Research Center, three-dimensional DSMC efforts concentrate on external flows around blunt bodies. Because of the considerable experience obtained with the two-dimensional wedge flows, the blunt-wedge corner flow has been chosen as the first three-dimensional flow problem for the application of the general three-dimensional DSMC program. The results of this study will be useful in understanding the flow around the wing-body junctures of space vehicles. Obviously, accurate aerothermal loading estimations are essential in designing the structures and materials of hypersonic vehicles.[11] Three-dimensional corner flow is a fundamental problem and has been studied in the past with various continuum methods. This is the first time that it has been studied using a particle approach.

Analysis

Direct simulation techniques are widely used today for various engineering applications. They provide good solutions for a range of problems, many of which are impossible to calculate with other methods. Direct simulation techniques are relatively easy to use, flexible, and have no stability problems; i.e., they can produce "a" solution under almost any circumstances. However, it is necessary to satisfy their requirements by selecting the computational parameters properly. Only when the computational approximations are kept within allowable bounds are meaningful results obtained. It should be noted that experience can play an important role in choosing the computational parameters properly in a short time.

This study concentrates on the corner flow at 85 and 100-km altitudes during re-entry. At these altitudes, the mean free paths of the gas molecules are fairly large, and the Knudsen numbers, based on the base height of the wedges, are of order $Kn_\infty \approx 0.2$ and 2, respectively. Clearly, these flows cannot be simulated using the Navier-Stokes equations because the continuum assumptions are violated. On the other hand, the Boltzmann equation is too cumbersome to apply. Consequently, from the computational point of view, the direct simulation techniques appear to be the most feasible methods for the simulation of these flows.

In this study, the DSMC method as developed by Bird is used to compute the flow in the transitional flight regime; i.e., flow that is bound by the continuum and free molecule limits. The DSMC method is a technique that models a real-gas flow by tracing some thousands of representative molecules whose position coordinates, velocity components, and internal states are stored in the computer. For computational convenience, the domain is divided into regions, and each region consists of a network of cells. In the three-dimensional DSMC applications, the cells are deformed hexahedra, and each cell is further divided into five tetrahedral subcells. The motion of the molecules in this domain is computed with small time intervals Δt_m, and after each time step the positions of the molecules are updated considering the possible interactions with the domain boundaries. In the DSMC method, the intermolecular collisions are uncoupled from the molecular motion over the time step Δt_m, and the number of intermolecular collisions appropriate for the time step is computed on a probabilistic basis within each cell. After the collisions, the velocity components and internal states of the colliding molecules are updated.

Bird[1] suggests that the cell sizes must be selected such that the change in flow properties across each cell becomes small, and Δt_m must be small compared with the mean collision time

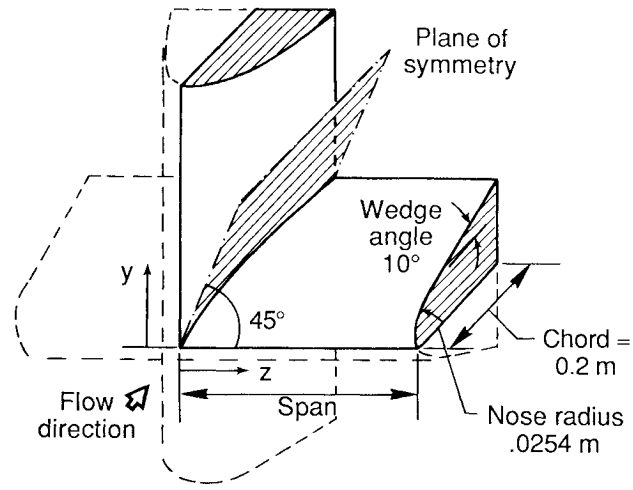

Fig. 1 Schematic of the body.

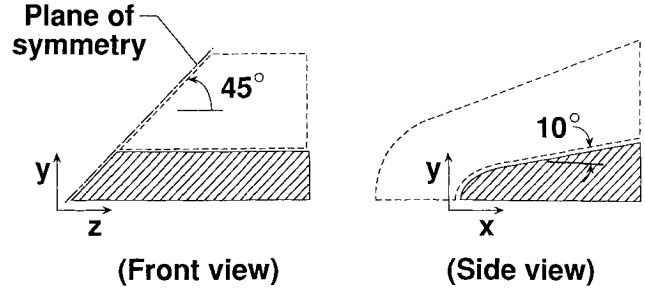

Fig. 2 Schematic of the computational domain.

per molecule. Also, the number of simulated molecules in each cell should be at least on the order of 10. The regions in the domain may be associated with different Δt_m values and weighting factors that specify the number of real molecules represented by each computational molecule.

The intermolecular collisions in this study have been modeled using the variable-hard-sphere (VHS) model[2] in which the molecules are treated as hard spheres, as far as the scattering is concerned, with collision cross sections that depend on the relative speed of the colliding partners. This model is being used in most of the DSMC applications today.

Computational Results

In this paper, computations for flow around two identical blunt wedges that intersect at a 90-deg angle are presented. The body has a nose radius of 0.0254 m, and the wedge angles are 10 deg. Figure 1 shows the schematic of the body. Clearly, there are four symmetric quadrants around the intersecting wedges, and because of the existence of a plane of symmetry within each quadrant, only half of a quadrant is considered in the numerical simulation. The computational domain is sketched in Fig. 2. Computations have been performed for flow in the transitional flight regimes encountered at 85 and 100-km altitudes during entry. The number density of air at 100 km is about 10 times smaller than that at 85-km altitude, and because the gas is more rarefied the disturbance field is much larger. Therefore, a bigger computational domain with larger cells is used at 100-km altitude. The domain lies between $x = -0.1$–0.2 m, $y = 0$–0.2 m, and $z = 0$–0.3 m for the 85-km altitude case, and between $x = -0.3$–0.2 m, $y = 0$–0.35 m, and $z = 0$–0.5 m for the 100-km altitude case.

The computational domains consist of regions lying on top of each other (like layers of pancakes) in the normal direction. For the 85 and 100-km altitude cases, 10 and 5 regions are used, respectively. For all cases, equal number of cells are used in the streamwise and spanwise directions, and the adjacent cells and subcells in neighboring regions are exactly matched.

For the 85-km altitude case, the computational domain is divided into 16 cells in the streamwise direction (8 along the nose and 8 on the wedge), 20 cells in the normal direction, and 16 cells in the spanwise direction. Figure 3 shows the body-fitted computational grid for the 85-km case. The broken lines show the other symmetric half of the quadrant and are drawn for visual aid only. The thick solid lines in this figure show the region boundaries. Of the 10 regions, only 7 can be easily seen in this figure. For the 100-km altitude case, there are 16 cells in the streamwise direction (6 along the nose and 10 on the wedge), 11 cells in the normal direction, and 8 cells in the spanwise direction.

At the freestream boundaries, atmospheric conditions for 85 and 100-km altitudes are used. Table 1 lists the atmospheric conditions at these altitudes. At the far end of the span, a specular boundary condition is imposed in the x-y plane. This can only be justified if the end of the span is sufficiently far from the intersection that the spanwise gradients are negligible. (The results discussed later indicate this to be the case.) Also, because of symmetry a specular boundary condition is used for the x-z plane at $y = 0$. The body surface temperature is assumed to be at a uniform 1000 K with full thermal accommodation and diffuse reflection for the gas-surface interactions. At the downstream boundary, a vacuum condition is imposed. Past experience has shown that if freestream conditions had been used rather than the vacuum boundary conditions the results would have differed only slightly due to the fact that supersonic velocities prevail in most of the exit flow.

As for the collisions of particles among themselves, the VHS model is used. Five chemical species (O_2, N_2, O, N, and NO) are present in the real-gas model, and energy exchange between translational and internal (rotational and vibrational) modes is considered during the collisions. Bird[12] has recently suggested that the collision partners be selected from the same tetrahedral subcells (rather than from the same cells) in order to improve the results in so far as the conversation of angular velocity of the collision partners is concerned (an issue raised by Meiburg[13]). Only when there is one particle in a subcell is the collision partner selected from an adjacent subcell. This procedure is implemented in the current computations, but the present results are not sensitive to the selection scheme since the cells are sufficiently small.

In this study, all of the three-dimensional computations have been performed on the CRAY-2 at NASA Ames. The two-dimensional programs and some of the small jobs requiring less than 1M words memory have been run on a Perkin Elmer 3250 dedicated computer at NASA Langley. The computations for the 85-km altitude case required 2.7M words computer memory and 20 h of total CPU run time, whereas the 100-km altitude computations are done using only 1M words computer memory and 4.4 h of total computational time on the CRAY-2.

In order to check the machine independency of the results, one of the three-dimensional cases has been run on both computers, and the results are in very good agreement. The three-dimensional program used in this study has not been written in a special form to make use of the fast vector operations available with the CRAY-2. For the particular case mentioned above, the CPU run time on the CRAY-2 is 30 times less than that on the Perkin Elmer.

Once steady state was achieved in the simulations, computations were carried out for an additional 4000 time steps, and samples were taken every other time step to arrive at the time-averaged results. The total number of simulated molecules

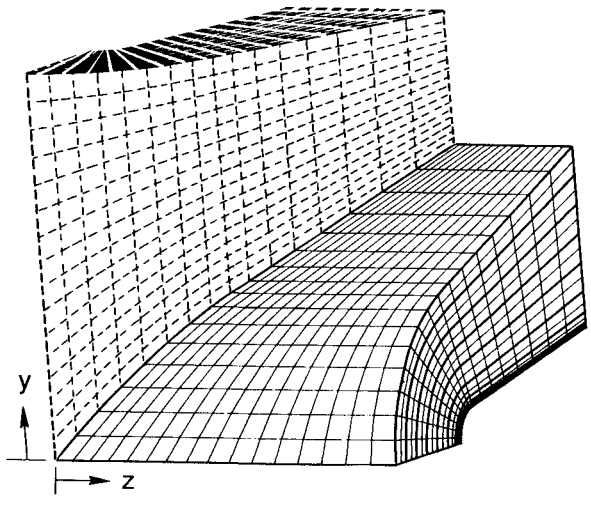

Fig. 3 Computational grid (alt = 85 km). (Thick solid lines show region boundaries. The broken lines show the other symmetric half of the quadrant for visual aid.)

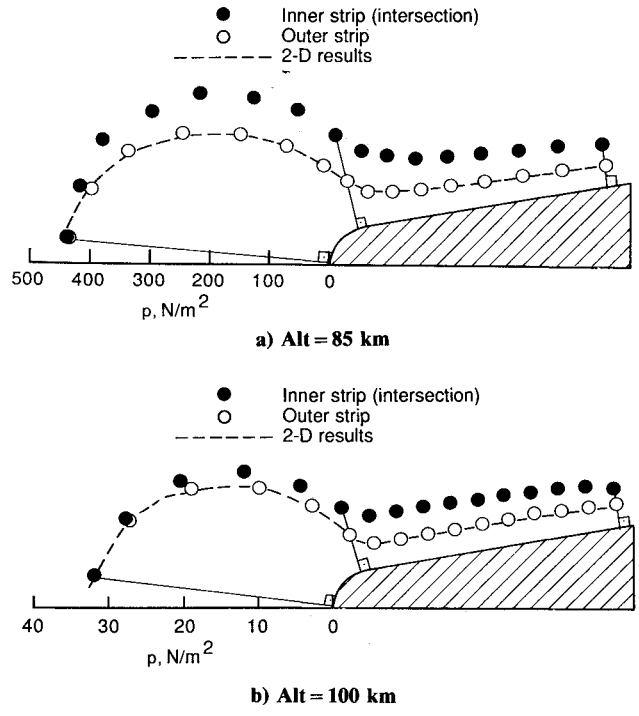

Fig. 4 Surface pressure distributions.

Table 1 Freestream conditions

Altitude, km	Density, kg/m^3	U_∞, km/s	T_∞, K	Mole fractions X_{O_2}	X_{N_2}	X_O	$\bar{M}$, g/mol	λ_∞, m
100	$(5.641)\ 10^{-7}$	7.5	194	0.177	0.784	0.039	28.24	$(1.37)\ 10^{-1}$
85	$(7.955)\ 10^{-6}$	7.5	181	0.237	0.763	0	28.95	$(9.94)\ 10^{-3}$

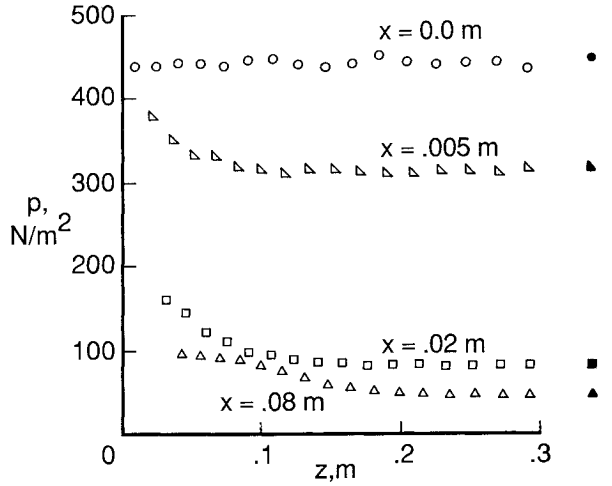

Fig. 5 Surface pressure distributions (alt = 85 km); two-dimensional results are shown by solid symbols.

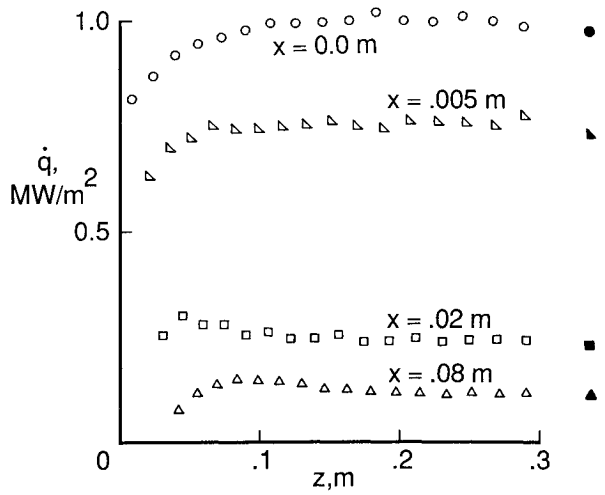

Fig. 8 Surface heat-transfer rate distributions (alt = 85 km); two-dimensional results are shown by solid symbols.

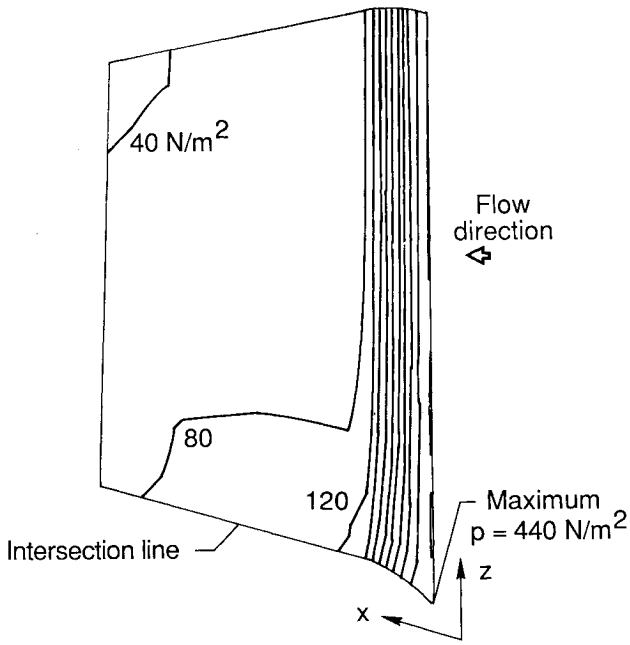

Fig. 6 Surface pressure contours (alt = 85 km).

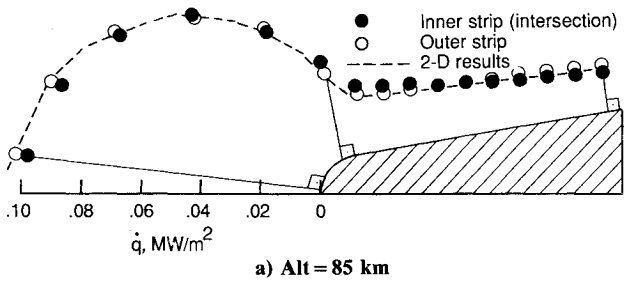

a) Alt = 85 km

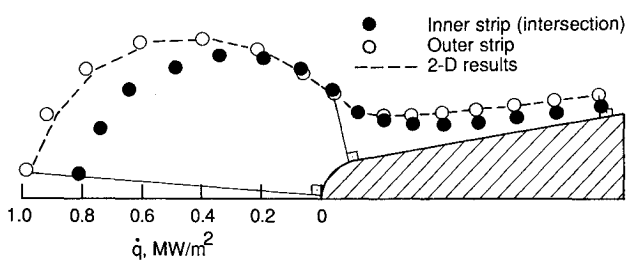

b) Alt = 100 km

Fig. 7 Surface heat-transfer rate distributions.

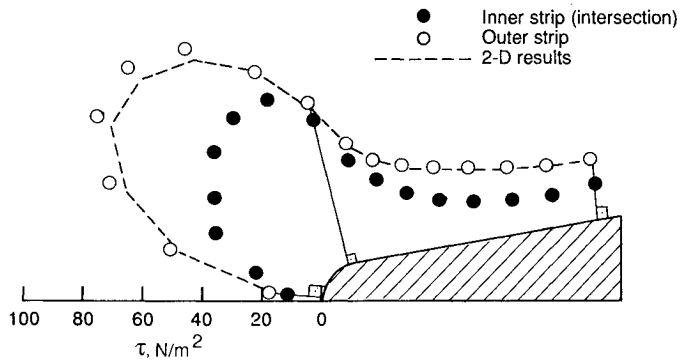

a) Alt = 85 km

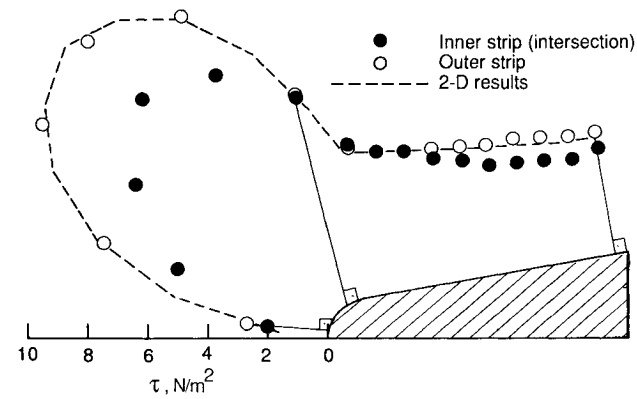

b) Alt = 100 km

Fig. 9 Surface shear stress distributions.

used for the 85-km case was 82,200, whereas the number for the 100-km case was 20,800. Examples of the time-averaged results are presented in Figs. 4–14. Surface pressure, heat-transfer rate, and shear stress distributions are shown in Figs. 4–9 for both the 85 and 100-km altitude cases. The surface shear stress (Fig. 9) is chosen to be the one parallel to the grid line in the streamwise direction. In Figs. 4, 7, and 9, the results are shown by perpendicular distances from the body surface. In these figures, "inner" and "outer" strips are the streamwise surface strips closest to and farthest from the wedge intersection, respectively.

In Figs. 10–14, various flowfield properties are presented. Figure 10 shows the flowfield density and translational temperature distributions along the stagnation streamlines for 85 and 100-km altitude cases. Again, the inner and outer stagnation lines are the ones closest to and farthest from the wedge intersection, respectively. Density distributions near the body

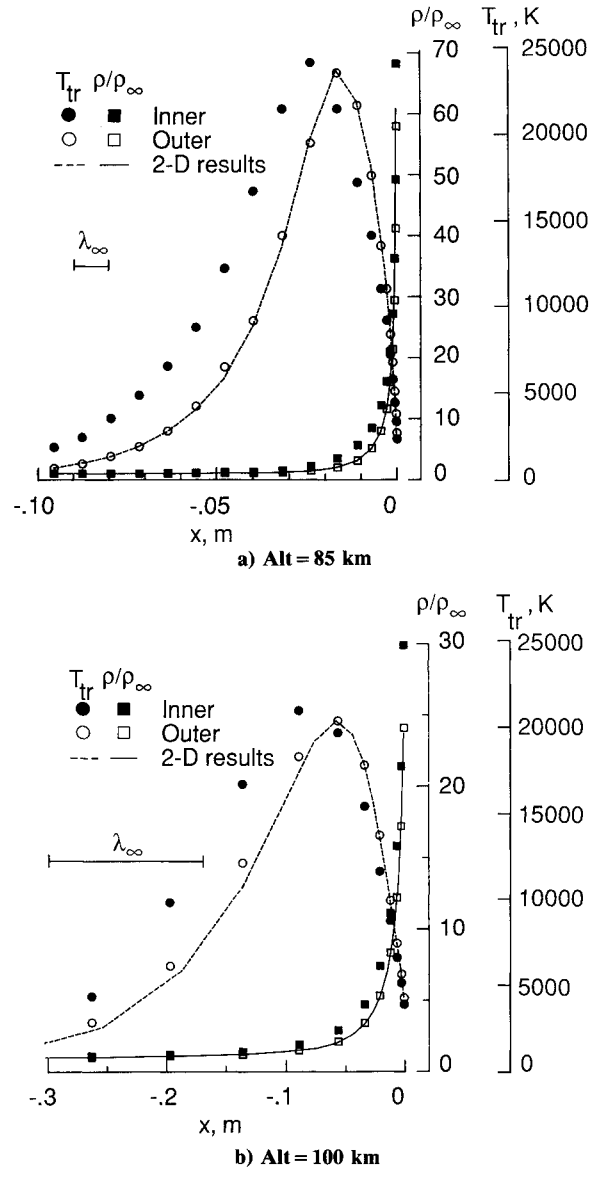

Fig. 10 Stagnation streamline density and translational temperature distributions.

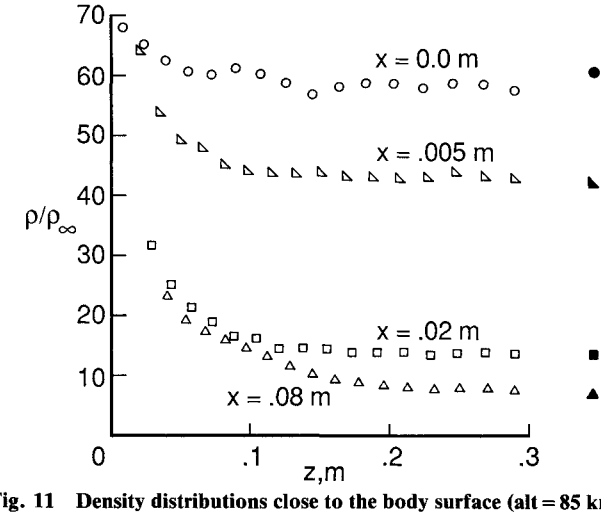

Fig. 11 Density distributions close to the body surface (alt = 85 km); two-dimensional results are shown by solid symbols.

surface (i.e., half-cell size away from the surface) are plotted in Figs. 11 and 12 for the 85-km altitude. For the same case, Fig. 13 shows the mass fraction distributions along the inner

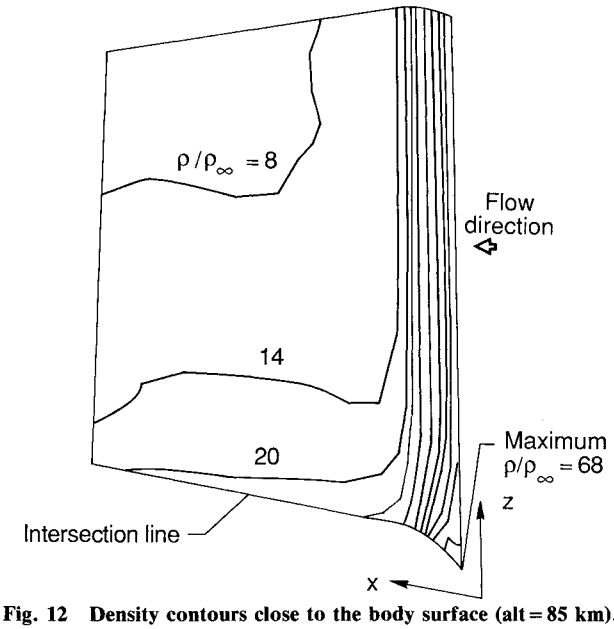

Fig. 12 Density contours close to the body surface (alt = 85 km).

and outer stagnation streamlines. The corresponding atomic oxygen mass fraction distributions near the body surface are presented in Fig. 14. Note that, along the wedge corner, the atomic oxygen mass fraction has its highest value and remains fairly constant along the intersection line, but at locations far away from the wall intersection, it drops both in the streamwise and spanwise directions.

At locations removed from the wedge intersection, the three-dimensional results are expected to approach the two-dimensional wedge flow results. In order to check if the computational domain is extended far enough in the spanwise direction, the three-dimensional outer strip results are compared with the two-dimensional wedge flow results in some of the figures. For the 85-km altitude case, the two-dimensional grid had the same cell structure in the streamwise and normal directions as the one used in the three-dimensional simulation. For the 100-km altitude case, the two-dimensional results are taken from Ref. 8 in which a finer grid with 20 cells in the streamwise direction and 17 cells in the normal direction is used.

Discussion

The results of this paper can be analyzed qualitatively through an analogous argument. Let us first assume that there is only one wedge in the flowfield. Clearly a two-dimensional flowfield will develop around the body. Now, let us introduce a second wedge that is intersecting with the first one at a 90-deg angle. How would the second wedge affect the results?

Before answering this question, let us look at the results of another comparative study[8,14] on the flows about two-dimensional wedges and axisymmetric cones that have the same nose radii and body half angles. That study shows that under identical freestream conditions, the bow shock produced by the wedge is located further upstream of the body than that produced by the cone, as one would expect. That is, the two-dimensional blunt wedge produces a much larger flowfield disturbance than the corresponding axisymmetric body. The results show that the wedge surface pressures and flow densities are higher, but the surface heat transfer and shear stresses are smaller than those on the corresponding axisymmetric blunt cone.

The analogous effect is evident in the present results where the double wedge body produces an even larger disturbance to the oncoming freestream than a single wedge. In other words, the presence of the second wedge effectively increases the overall bluntness of the body. The computational results for both 85 and 100-km altitudes show that along the stagnation

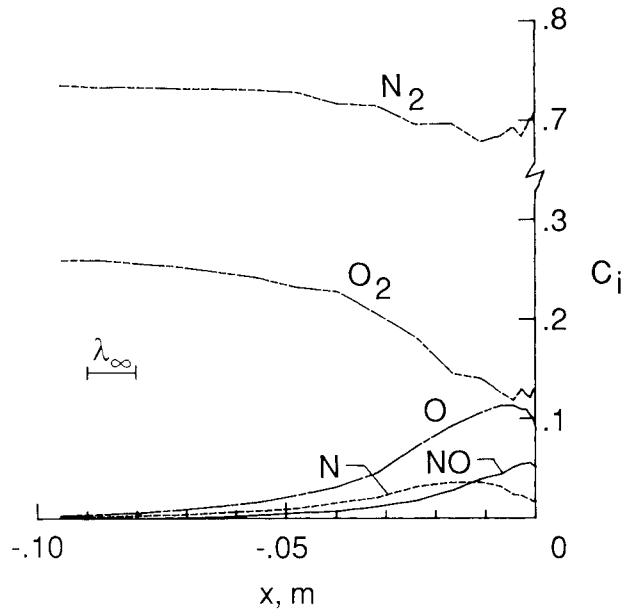

a) Inner stagnation streamline

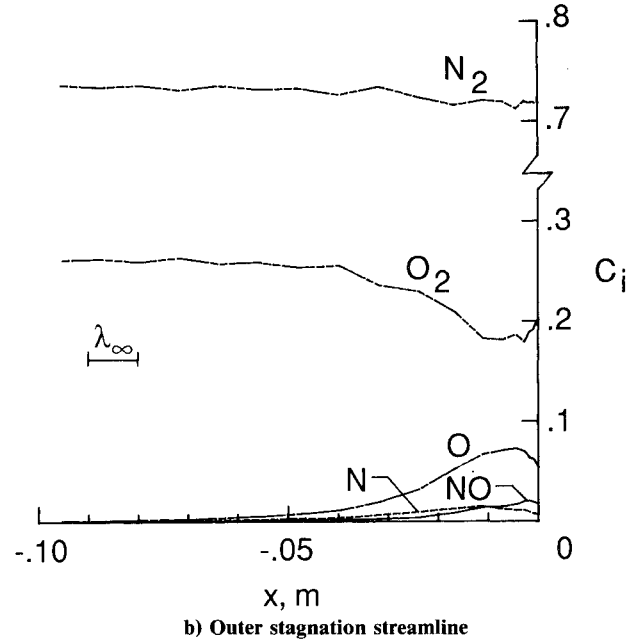

b) Outer stagnation streamline

Fig. 13 Mass fraction distributions along stagnation streamlines (alt = 85 km).

streamlines the density, temperature, and velocity fields extend 25 to 35% more in front of the double wedge body than those in front of the single wedge body. The flowfield structure and surface quantities resulting from the interaction of the two wedges (inner streamwise strip) as compared to that well removed from the intersection (outer streamwise strip) have a qualitative behavior similar to that observed between the two-dimensional wedge and axisymmetric cone results; i.e., the surface pressures and flow densities are higher, but the surface heat transfer and shear stresses are lower for the inner strip than those calculated for the outer strip.

This is the first application of a general three-dimensional DSMC program at NASA Langley. And so, in order to build confidence in the computational results, the three-dimensional program has been applied to three test flow cases for which solutions are already known. In these cases, the angle between the oblique symmetry plane and the x-z plane has been increased to 90 deg, and only one cell is placed in the spanwise direction. In other words, the three-dimensional program is forced to produce two-dimensional results.

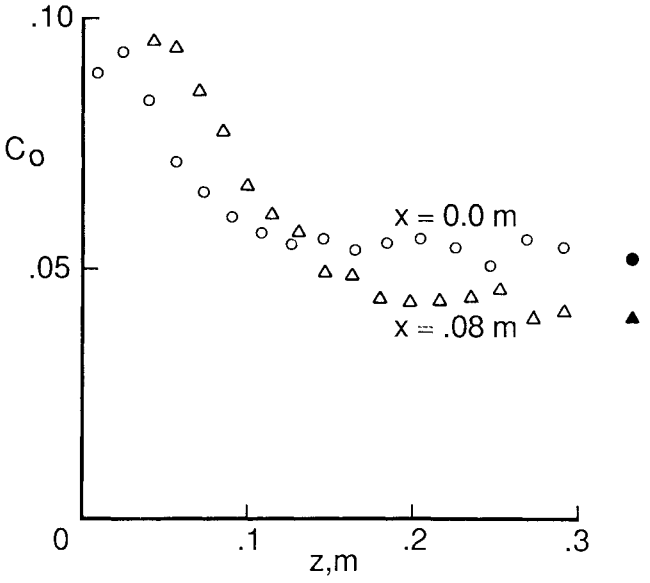

Fig. 14 Atomic oxygen mass fraction distributions close to the body surface (alt = 85 km); two-dimensional results are shown by solid symbols.

In the first test problem, a freestream boundary condition was imposed on the body surface. In this case, a uniform freestream flow did develop everywhere in the whole flowfield.

In the second test problem, the molecules were allowed to move freely in the computational domain without colliding among themselves, i.e., a collisionless flow was developed. In this case, the results were found to be in excellent agreement with those of the theoretical free molecule flow limit.

In the third test problem, the two-dimensional wedge flow results produced by the three-dimensional program were compared with those produced by a separate two-dimensional program. The results, again, were in excellent agreement.

Apart from these test cases, the three-dimensional solutions themselves approach the two-dimensional wedge flow solutions at locations sufficiently far away from the wedge intersection as shown in Figs. 4–7. Naturally, all of these results help to produce more confidence in the three-dimensional results.

In order to produce grid-independent three-dimensional results, various grids with different cell sizes need to be tested in the computations. In this study, this was achieved by making use of the corresponding two-dimensional program. Results show that the three-dimensional solutions do approach the two-dimensional solutions at locations removed from the wedge intersection. Therefore, the cell sizes in the normal and streamwise directions can be determined (at least in that part of the domain) through the use of the two-dimensional program. Later, the three-dimensional program can be used to determine the cell sizes in the spanwise direction only. This scheme, although not perfect, is much quicker than repeating the three-dimensional computations with finer cells in all three directions, and for the 85-km altitude case, it was the only viable alternative because a finer grid with more than $16\times20\times16$ cells would have been very demanding because of its CPU time requirement.

For the 85-km altitude case, the two-dimensional results with 16×20 cells are in good agreement with those of Ref. 8 in which a much finer grid with 20×70 cells was used. The $16\times20\times16$ cell grid has roughly the minimum number of cells for the 85-km case. The cell sizes in the normal direction are approximately equal to the local mean free path. In our early computations, we tried a crude grid with $8\times7\times8$ cells. This crude grid produces excellent results for the surface pressure and flowfield densities. However, it overpredicts the surface heat transfer and shear stress all along the inner strip and

underpredicts the flowfield temperatures at locations far away from the surface.

The grid independency test has also been applied to the 100-km altitude case. At this altitude, because the air is much more rarefied, the $16 \times 11 \times 8$ grid yields cell sizes in the normal direction that are about one-third of the local mean free path. Because this grid is already fine enough, somewhat coarser grids were tried in all directions using both two- and three-dimensional programs, and the results were found to be not affected.

Unfortunately, at the present there are no experimental data available to be compared with the computational results of this study. The only experimental data that would indirectly support these three-dimensional results are the heat-transfer data obtained by Boylan[15] for the flow around a two-dimensional wedge. Cuda and Moss[8] show that their two-dimensional results are in excellent agreement with these data under the same freestream conditions. The only consolation is that the present three-dimensional results are in good agreement with their two-dimensional computations. It should also be noted as a final point that the geometry used in this work is not a particularly complicated one, and in the future an experiment could be easily performed in a laboratory for lower energy flow conditions.

Summary and Conclusions

Using the DSMC method, the three-dimensional flow about two wedges intersecting at a 90-deg angle has been computed for the transitional regime encountered at 85 and 100-km altitudes during a simulated re-entry.

The computational results show the following:

1) The disturbance field produced by the double wedge is larger than that produced by a single wedge.

2) Near the wedge intersection, the surface pressures and densities are higher, but the surface heat transfer and shear stresses are smaller as compared with those at locations far away from the wedge intersection.

3) At 85-km altitude, dissociation is important and O, N, and NO concentrations are significant near the wedge intersection. For this particular application, dissociation is negligible at 100-km altitude.

4) The three-dimensional results approach monotonically the two-dimensional wedge flow results in the spanwise direction.

For this particular problem, the application of the three-dimensional DSMC method at altitudes lower than 85 km is prohibitively difficult due to CPU time requirements. It seems that currently most of the three-dimensional DSMC applications are appropriate only for high altitudes even with today's supercomputers. For users who use supercomputers about an hour a day for problems requiring about 3 or 4M words computer memory, dedicated minicomputers provide an inexpensive alternative if they are used continuously. One thing is also clear: with the start of the development of the three-dimensional codes, experimental data are urgently needed for code validation.

This is the first application of a general three-dimensional DSMC program to a three-dimensional flow problem at the NASA Langley Research Center. In the meantime, parallel efforts are underway to apply the three-dimensional code to other configurations such as the Aeroassist Flight Experiment (AFE) vehicle.

References

[1]Bird, G. A., *Molecular Gas Dynamics,* Clarendon Press, Oxford, England, 1976.

[2]Bird, G. A., "Monte-Carlo Simulation in an Engineering Context," *AIAA Progress in Astronautics and Aeronautics: Rarefied Gas Dynamics,* Vol. 74, Pt. 1, edited by Sam S. Fisher, AIAA, New York, 1981, pp. 239–255.

[3]Moss, J. N. and Bird, G. A., "Monte Carlo Simulations in Support of the Shuttle Upper Atmospheric Mass Spectrometer Experiment," *Journal of Thermophysics and Heat Transfer,* Vol. 2, No. 2, April 1988, pp. 138–144.

[4]Moss, J. N. and Bird, G. A., "Direct Simulation of Transitional Flow for Hypersonic Re-entry Conditions," *Progress in Astronautics and Aeronautics: Thermal Design of Aeroassisted Orbital Transfer Vehicles,* Vol. 96, edited by H. F. Nelson, AIAA, New York, 1985, pp. 113–139.

[5]Bird, G. A., "Low-Density Aerothermodynamics," *Progress in Astronautics and Aeronautics: Thermophysical Aspects of Re-Entry Flows,* Vol. 103, edited by J. N. Moss and C. D. Scott, AIAA, New York, 1986, pp. 3–24.

[6]Dahlen, G. A., Macrossan, M. N., Brundin, C. L., and Harvey, J. K., "Blunt Cones in Rarefied Hypersonic Flow; Experiments and Monte-Carlo Simulations," *Proceedings of the 14th International Symposium on Rarefied Gas Dynamics,* Vol. 1, edited by H. Oguchi, University of Tokyo Press, Tokyo, Japan, 1984, pp. 229-240.

[7]Harvey, J K., "Direct Simulation Monte Carlo Method and Comparison with Experiment," *Progress in Astronautics and Aeronautics: Thermophysical Aspects of Re-Entry Flows,* Vol. 103, edited by J. N. Moss and C. D. Scott, AIAA, New York, 1986, pp. 25–43.

[8]Cuda, V., Jr., and Moss, J. N., "Direct Simulation of Hypersonic Flows Over Blunt Wedges, *Journal of Thermophysics and Heat Transfer,* Vol. 1, No. 2, April 1987, pp. 97–104.

[9]Bird, G. A., "Direct Simulation of Typical AOTV Entry Flows," AIAA Paper 86-1310, June 1986.

[10]Harvey, J. K., Celenligil, M. C., Dominy, R. G., and Gilmore, M. R., "A Flat-Ended Circular Cylinder in Hypersonic Rarefied Flow," AIAA Paper 89-1709, June 1989.

[11]Jackson, L. R., Dixon, S. C., Tenney, D. R., Carter, A. L., and Stephens, J. R., "Hypersonic Structures and Materials: A Progress Report," *Aerospace America,* Vol. 25, No. 10, Oct. 1987, pp. 24–30.

[12]Bird, G. A., "Direct Simulation of Gas Flows at the Molecular Level," *Proceedings of the First World Congress on Computational Mechanics,* Univ. of Texas at Austin, Austin, TX, Sept. 1986.

[13]Meiburg, E., "Direct Simulation Techniques for the Boltzman Equation," Rept. DFVLR-FB 85-13, Institut fur Theoretische Stromungsmechanik der DFVLR, Goettingen, Federal Republic of Germany 1985.

[14]Moss, J. N., Cuda, V., and Simmonds, A. L., "Nonequilibrium Effects for Hypersonic Transitional Flows," AIAA Paper 87-0404, Jan. 1987.

[15]Boylan, D. A., "Laminar Convective Heat-Transfer Rates on a Hemisphere Cylinder in Rarefied Hypersonic Flow," *AIAA Journal,* Vol. 9, Aug. 1971, pp. 1661–1663.